JPE 13-4-3

http://dx.doi.org/10.6113/JPE.2013.13.4.528

Traction Motor-Inverter Utilized Battery Charger for PHEVs

Dong-Gyun Woo*, Yun-Sung Kim*, Gu-Bae Kang**, and Byoung-Kuk Lee†

*†College of Information & Communication Eng., Sungkyunkwan University, Suwon, Korea
** Research & Development Division, Hyundai Motor Company, Hwasung, Korea

Abstract

Most eco-friendly cars can adopt the concept of an integrated battery charger (IBC), which uses currently available motor drive systems. The IBC has a lot of strong points such as low cost and minimum space for the high voltage battery charger. On the other hand, it also has some defects caused by its structure. In this paper, the shortcomings of the conventional IBC for PHEVs with interior permanent magnet motors are discussed, and two advanced IBCs with improved performance are presented. Compared with the conventional IBC, the two advanced IBCs have plenty of strengths such as low common noise, high efficiency, simple sensing methods, etc. Then, the digital control algorithm is modified and a power loss calculation is carried out with simulation software. Finally, experimental results are provided to show the performance of the IBC systems.

Key words: Battery charger, PFC control algorithm, Plug-in hybrid electric vehicle, Traction motor

I. INTRODUCTION

For the past several years, the EU has been tightening the mandatory restrictions on the emissions of carbon dioxide with an aim to cut CO_2 and other greenhouse gases. To meet these CO_2 emission standards, several car manufacturers have been working on the development of various eco-friendly cars like hybrid electric vehicles (HEVs), plug-in hybrid electric vehicles (PHEVs), and electric vehicles (EVs). In these vehicles, the high voltage battery pack plays a vital role as an energy source for the electric propulsion and a large amount of accessory equipment. Therefore, the technology related to battery packs is being considered as the core technology in the green car field.

For charging a battery pack without damaging it, many types of battery chargers have been introduced to the market. In general, battery chargers are classified into the on-board type and the stand-alone type [2]. However, both types have disadvantages in terms of cost, weight, and volume. Hence, integrated battery chargers (IBC) with a novel concept that utilize currently available power conversion hardware have been proposed [1]-[5]. In these chargers, a 3-phase inverter and a M/G (motor and generator) operate together as a boost power factor correction (PFC) converter. Compared with other battery chargers, the IBC has outstanding merits in terms of cost, weight, and volume.

IBCs can be applied to HEVs, PHEVs, and EVs. Among these vehicles, the PHEV is being regarded as a viable candidate for short daily commutes [5]. PHEVs offer a relatively long all electric range (AER) (e.g. 20~40 miles) owing to a relatively high battery capacity. Some studies have been conducted on the IBC for PHEVs [3], [5]. The authors of [3] used two inverters and two M/Gs for battery charging operation and the neutral points of both M/Gs were connected with a grid in series. In order to make the phase currents of the M/Gs identical, a simple synchronous switching control algorithm was employed. In [5], the interleaved pulse width modulated (PWM) technique was applied to the same hardware system as that used in [3]. This study verified that interleaved PWM switching offers better performance than synchronous PWM switching and hysteresis switching. Meanwhile, the conventional IBC in [3] and [5] has some drawbacks such as high common mode (CM) noise, unnecessary loss generation, complex input voltage sensing, inaccurate input current calculation, etc.

This paper is arranged as follows: Section II explains and suggests the system configuration of IBCs for PHEVs; Section III introduces a modified system control algorithm; Section IV calculates power losses of the three IBCs using a simulation tool; Section V gives experimental results and evaluates the performance of the three IBCs; and Section VI draws some conclusions.

Manuscript received Jan. 28, 2013; revised Mar. 25, 2013
Recommended for publication by Associate Editor Jin Hur.
†Corresponding Author: bkleeskku@skku.edu
Tel: +82-31-299-4581, Fax: +82-31-299-4612, Sungkyunkwan University
*College of Information & Comm. Eng., Sungkyunkwan Univ., Korea
**Research & Development Division, Hyundai Motor Company, Korea

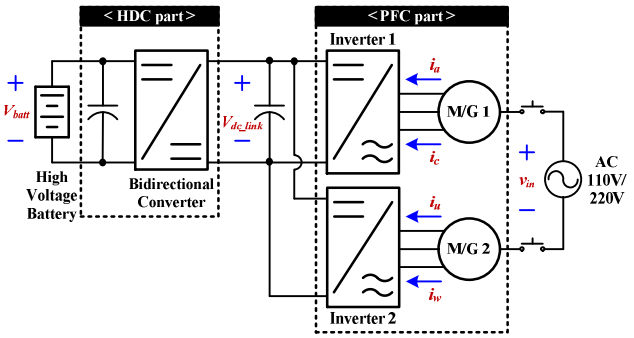

Fig. 1. System configuration of the conventional IBC for PHEVs.

II. SYSTEM CONFIGURATION

Fig. 1 presents the system configuration of a conventional IBC for PHEVs. It consists of a HDC part and a PFC part, power components for the ac motor drive [3], [5]: Two M/Gs, two 3-phase inverters, a bidirectional converter, and a high voltage battery pack. Only two mechanical switches are added to connect the center taps of each M/G to the grid. As a result, the conventional IBC has many strong points: It can minimize system volume and weight; it is able to reduce the cost of the on-board battery charger; it can use any household utility outlet to charge the battery pack. However, there are some problems and limits when this system is implemented: 1) switching frequency; 2) power loss; 3) CM noise; 4) power rating of the propulsion system; 5) input voltage and input current sensing; 6) motor inductance. These considerations are described below in detail.

First, this system has a limitation on the switching frequency. Most inverter systems for traction motor drive applications adopt IGBT modules. In general, the maximum switching speed of the IGBT modules in propulsion inverters is about 20kHz. This means that the switching frequency for the boost PFC control in the PFC part is also limited to the maximum value. Fortunately, due to the three phase structure of inverters and M/Gs, the interleaved PWM switching technique can be employed in the PFC part without installing additional power components [5]. This switching technique has a lot of advantages. The modulation frequency of the input and output currents is three times higher than the switching frequency [4]; it results in higher input PF, lower input current total harmonic distortion (THD), and higher system efficiency.

Fig. 2 shows the power flow of the PFC part with an equivalent circuit. In each half line cycle, one combination of a M/G and an inverter operates as a boost PFC converter, and the other combination provides the current path between the negative terminal of the output and the ac grid. For example, during modes 1 and 2, a positive half line cycle, the bottom IGBTs of inverter 1 work as active switches and the bottom anti-parallel diodes of inverter 2 are turned on. Here, the current always flows through the three phase windings of M/G 2 and the bottom anti-parallel diodes of inverter 2. This

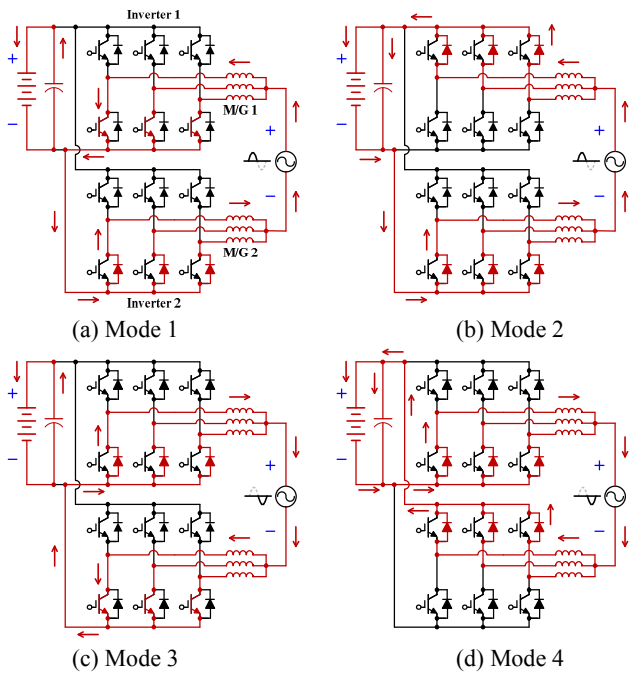

Fig. 2. Operating modes of the PFC part in the conventional IBC.

results in unnecessary conduction losses. Likewise, conduction losses occur in M/G 1 and inverter 1 during modes 3 and 4, a negative half line cycle. It is necessary to reduce these power losses to improve the system efficiency.

In the PFC part, there are two kinds of parasitic capacitances [8]: 1) C_c between the collector of each bottom IGBT in the inverters and the earth ground; 2) C_g from the output ground to the earth ground. During the charging operation, the output ground pulsates with a high frequency, switching frequency, because the output ground is connected to the ac grid via a motor (M/G 1 or M/G 2), and the amplitude is almost half of the high output voltage [6], [8]. The dv/dt on the parasitic capacitors results in a CM noise current flowing through each of the parasitic capacitors. Since C_g is normally much larger than C_c, C_g is the main factor of the CM noise in this system [6]. This high conducted CM electromagnetic interference (EMI) noise needs to be minimized; otherwise a large CM choke has to be applied so as to meet the electromagnetic compatibility (EMC) standards.

The IBC system can be used for lower powers (e.g. < 6.6kW) such as on-board type or higher powers (e.g. ≥ 40kW) like the stand-alone type. Assuming the power rating of M/G 2 and inverter 2 is lower than that of M/G1, inverter 1, and a bidirectional converter, the charging power is limited by the maximum power rating of M/G 2 and inverter 2 [3]. For instance, if an ac source with higher power rating than M/G 2 and inverter 2 is used for quick charging, the charging power should be kept below their rating. Besides, high power rating of the propulsion system has a bad impact on the

charging efficiency. When a household utility outlet is utilized as the ac power source, the system efficiency might be relatively low owing to the large difference in the power rating between the propulsion system and the household ac grid.

In order to generate the input current reference for the average current mode control in the PFC part, the input voltage, v_{in}, in Fig. 1 has to be sensed. There are some useful ways to sense input voltage, such as the voltage divider, line frequency transformer, optocoupler, and so on [7]. In this system, the voltage divider can not be employed for input voltage sensing because the voltage potential of the output ground is different from that of the input terminals. In other words, isolation is an essential factor in sensing the input voltage. The line frequency transformer can obtain isolation. However, it increases system volume, weight and cost. Accordingly, it is not recommended for the IBC system. In the market, there are many kinds of integrated circuits (ICs) including the optocoupler for isolation like isolation amplifiers. They provide the precision and stability needed to accurately monitor the current or voltage in high noise environments. Therefore, the optocoupler is the best solution for input voltage sensing in the conventional IBC.

In general PHEV systems, most inverters for the motor drive sense just two phase currents because it is possible to synthesize the other one with the information from both currents. For this reason, in the conventional IBC, only two phase currents are provided to compute the input current. However, in real systems, three phase currents are not identical due to various factors such as the motor structure, control method, parasitic components, etc. Moreover, if the current transducer (CT) in an inverter module is used for low power charging (e.g. 3.3kW), the current resolution becomes considerably low. As a result, there is a gap between the actual input current and the estimation value. This difference can have an adverse effect on the control accuracy. In order to solve this problem, a CT or a hall IC should be added between the ac grid and either M/G 1 or M/G 2.

Lastly, motor inductance should be checked whether it is enough to carry out the boost PFC control. The critical inductance value for the boost PFC operation is as follows:

$$L_{crit} = \frac{\sqrt{2}V_{in(\min)}\left[1-\left(V_{in(\min)}/V_{out}\right)\right]}{\Delta I \times f_{sw}} \quad (1)$$

where L_{crit} is the critical inductance, $V_{in(\min)}$ is the minimum input ac voltage, V_{out} is the output dc voltage, $\triangle I$ is the maximum allowed current ripple, and f_{sw} is the switching frequency. If the motor inductance is lower than L_{crit}, the additional inductor must be installed between the neutral point of each M/G and the grid. For example, when the interior permanent magnet synchronous motor (IPMSM) in

TABLE I
SPECIFICATION OF THE M/G

Type	Interior PMSM
Maximum Power	9 kW
Rated Power	6.7 kW
Maximum Torque	45.3 N·m
Rated Torque	16.6 N·m
L_d, L_q	0.75mH, 1.73mH @ $10A_{rms}$

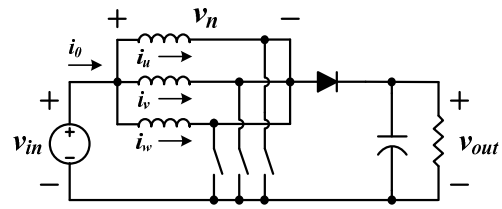

Fig. 3. Test circuit diagram for the measurement of motor inductances.

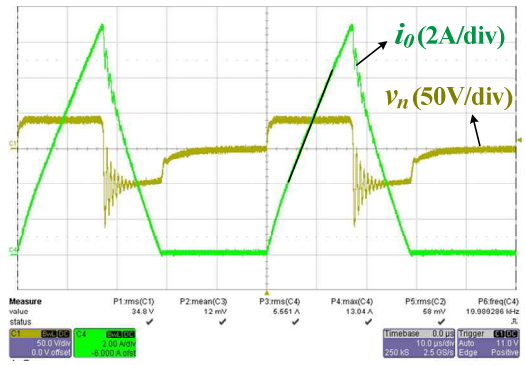

Fig. 4. Experimental waveforms under the synchronous PWM switching control (10.0μs/div).

Table I is considered for the M/Gs, the common mode inductance (L_{cm}) of the IPM motor can be estimated from experimentation [4]. Fig. 4 displays experimental waveforms under the synchronous PWM switching control from the test circuit configuration of Fig. 3. L_{cm} at 20kHz is 57.6μH. However, this might be too low to convert the ac grid voltage to a high battery voltage. Of course, this depends on the type and rated power of the M/G in the PHEVs. In order to prepare for a bad situation, this paper supposes that the IPM motor of Table I is employed for M/G 1 and M/G 2 in the PHEV system. Therefore, an additional inductor is required to meet the charging performance.

The above problems of the conventional IBC can be solved by modifying the structure of the PFC part in Fig. 1. Fig. 5 presents two advanced IBCs for PHEVs. Since the HDC part in each IBC is the identical to the one in Fig. 1, they are omitted here. They use an additional inductor for the purpose of compensating the small L_{cm}.

An IBC with a diode bridge is introduced in Fig. 5(a). In this case, the maximum charging power depends on the rated power of the propulsion system used to charge the high

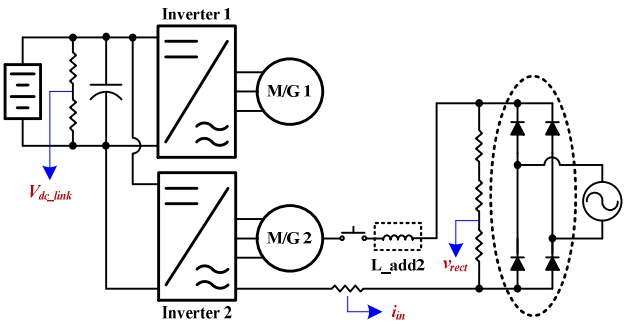

(a) IBC with a diode bridge

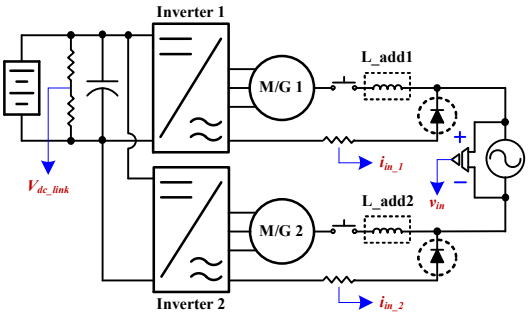

(b) IBC with two diodes

Fig. 5. System configuration of the advanced IBCs for PHEVs.

voltage battery. The charging power should be considered when choosing where to place the diode bridge.

In Fig. 5(a), only the parasitic capacitances between the collector of each of the bottom IGBTs and the earth ground influence the CM noise. This is because the output ground is always connected to the input terminal through the diode bridge. Thus the IBC with a diode bridge can reduce the CM noise [8]. In addition, input voltage sensing and input current sensing can be simplified by using a voltage divider and a shunt resistor, respectively.

The IBC with a diode bridge needs just one additional inductor, $L_{\_add2}$. However, the inductance should be twice that in the conventional IBC for the same input current ripple. During the charging operation, the two diodes of the diode bridge produce conduction losses while the unnecessary conduction losses on the return path of the input current disappear.

Fig. 5(b) shows an IBC with two additional diodes, which are slow recovery diodes. It can decrease the CM noise because the two additional diodes provide a low-frequency path. Moreover, it carries out the input current sensing with only two shunt resistors. The conduction loss on the return path of the input current is generated from just one of the additional diodes. However, in order to ensure the same input current ripple, the inductances of both additional inductors, $L_{\_add1}$ and $L_{\_add2}$, have to be two times higher than that in the conventional IBC.

III. CONTROL ALGORITHM

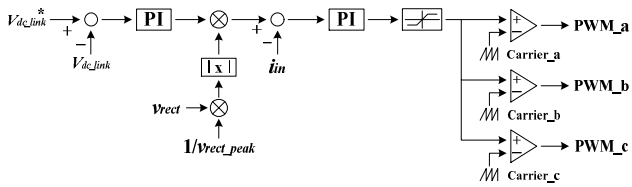

(a) Conventional average current mode control.

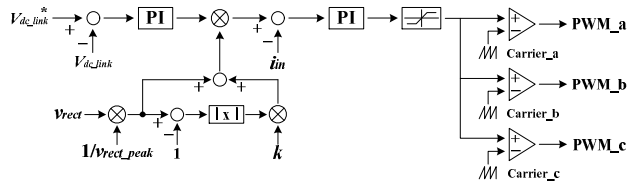

(b) Average current mode control with compensation function.

Fig. 6. Control block diagrams for the PFC part during positive half line cycle.

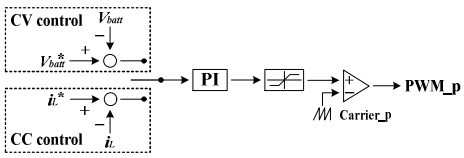

Fig. 7. Control block diagram for the HDC part.

A digital controller for propulsion is also used to charge the high voltage battery pack. For the charging mode, the PFC part operates like a boost PFC converter using the average current mode control. In digital implementation, the conventional average current mode control of Fig. 6(a) shows a somewhat lower PF performance when compared with analog controlled PFC systems. To improve this control method, a compensation method is proposed in Fig. 6(b). Here, the compensation constant k could be selected within a range of 0 to 0.5. As the constant k increases, the input current reference of the inner control loop at the zero crossing point of the input voltage also rises.

Fig. 7 presents a control block diagram for the HDC part which functions as a buck converter. There are two control modes which are the constant voltage (CV) control and the constant current (CC) control. The appropriate control mode needs to be selected to charge a high voltage battery without damaging it.

IV. POWER LOSS ANALYSIS

In order to analyze the power losses of the conventional IBC and the advanced IBCs, this paper uses the PSIM 9.0 simulation tool. It provides a thermal module option which can estimate device conduction losses and switching losses in a very short time. The loss calculation for the HDC part is not carried out because they do not have any differences.

Using the device database editor, the semiconductor device datasheet information is added into a database. The information is as follows: absolute maximum ratings,

electrical characteristics, thermal characteristics, etc. In this simulation, inverter 1 and inverter 2 are implemented with CP25TD1-24A IGBT modules, and the additional diode bridge and the two diodes are conducted with LL25XB60 bridge diodes. Then, the device information is loaded from the device database into the thermal modules.

The thermal module calculates the diode losses as follows:

$$\text{(Conduction loss)} = V_d \times I_d \tag{2}$$

$$\text{(Turn-off loss)} = E_{rr} \times f_{sw} \times \left(V_R / V_{R\_datasheet}\right) \tag{3}$$

$$= (1/4) \times Q_{rr} \times V_R \times f_{sw} \tag{4}$$

$$= (1/8) \times t_{rr} \times I_{rr} \times V_R \times f_{sw} \tag{5}$$

where V_d is the diode voltage drop, I_d is the diode forward current, E_{rr} is the reverse recovery energy losses, V_R is the reverse blocking voltage, $V_{R\_datasheet}$ is the reverse blocking voltage in the E_{rr} characteristics of the datasheet, Q_{rr} is the reverse recovery charge, t_{rr} is the reverse recovery time, and I_{rr} is the peak reverse recovery current. The diode turn-on losses are not considered. In addition, the IGBT losses are calculated as follows:

$$\text{(Conduction loss)} = V_{ce(sat)} \times I_c \tag{6}$$

$$\text{(Turn-on loss)} = E_{on} \times f_{sw} \times \left(V_{cc} / V_{cc\_datasheet}\right) \tag{7}$$

$$\text{(Turn-off loss)} = E_{off} \times f_{sw} \times \left(V_{cc} / V_{cc\_datasheet}\right) \tag{8}$$

where $V_{ce(sat)}$ is the saturation voltage, I_c is the collector current, E_{on} is the turn-on energy losses, V_{cc} is the actual dc bus voltage, $V_{cc\_datasheet}$ is the dc bus voltage in the E_{on} and E_{off} characteristics of the datasheet, and E_{off} is the turn-off energy losses. The loss calculation for the anti-parallel diodes is the same as (2)-(5). Therefore, the conduction losses and switching losses from the inverters, the two additional diodes, and the additional diode bridge are calculated by the thermal modules.

In addition, it is possible to calculate the inductor losses such as the copper loss and the core loss using some of the function blocks provided in PSIM. In this paper, High Flux cores are selected for the additional PFC inductors in the three IBCs. The inductances of $L_{\_add2}$ in Fig. 5(a) and $L_{\_add1}$ and $L_{\_add2}$ in Fig. 5(b) are designed at 1.2mH. Under the same conditions, the conventional IBC requires two additional inductors like those in Fig. 5(b). However, each of the inductances is one half of $L_{\_add1}$ or $L_{\_add2}$ in Fig. 5(b), 600μH. The inductor losses are calculated as follows:

$$\text{(Copper loss)} = I_{L(rms)}^2 \times R_c \tag{9}$$

$$\text{(Core loss)} = k_1 \times B^{k_2} \times f_{sw}^{k_3} \times V_L \tag{10}$$

where $I_{L(rms)}$ is the inductor rms current, R_c is the wire wound resistance, B is the flux density, and V_L is the core volume. k_1, k_2, and k_3 are coefficients depending on the inductor core. In the simulation, the measured R_c of the IPM motors and the designed inductors is used for the copper loss calculation. The core losses from M/G 1 and M/G 2 are neglected because the core losses from the motors in the three IBCs are approximately equal and it is difficult to get the information for the variables in (10).

TABLE II

SPECIFICATION OF THE SIMULATION

Input Voltage	220 Vac
Output Voltage	400 V
Input Frequency	60 Hz
Switching Frequency	20 kHz
Output power	3.3 kW

TABLE III

CALCULATED POWER LOSSES OF THE PFC PART IN THREE IBCS

Component	Loss (W)		
	Conventional IBC	IBC with a diode bridge	IBC with two diodes
Inverter 1	36.64	x	28.70
Inverter 2	36.58	57.12	28.62
M/G 1	24.44	x	15.82
M/G 2	24.44	31.77	15.82
Diode bridge	x	24.61	x
Two diodes	x	x	11.99
L_add1	7.73	x	6.13
L_add2	7.73	12.29	6.13
Total power loss	137.56	125.79	113.21

Table III presents the loss calculation results through the simulation under the specifications of Table II. The major loss factors in the conventional IBC are the IGBT switching losses (38.7W) and the anti-parallel diode conduction losses (27.2W) from the inverters and the copper losses (48.9W) of the motors. In the advanced IBCs, the anti-parallel diode conduction losses and the motor's copper losses are improved, but conduction losses occur in the additional diode bridge or in the two additional diodes. Between the two advanced IBCs, the IBC with two diodes has a lower total power loss because the loss from its two diodes is half the loss from the diode bridge. As a result, it can be predicted that the IBC with two diodes has the lowest total power loss among the three IBCs.

V. EXPERIMENTAL RESULTS

Fig. 8 shows a prototype which consists of a 35kW inverter 1, a 20kW inverter 2, a 20kW bidirectional dc-dc converter, and 6.7kW IPM motors. The boost PFC control and the buck control are implemented in a TMS320F28335PGFA DSP.

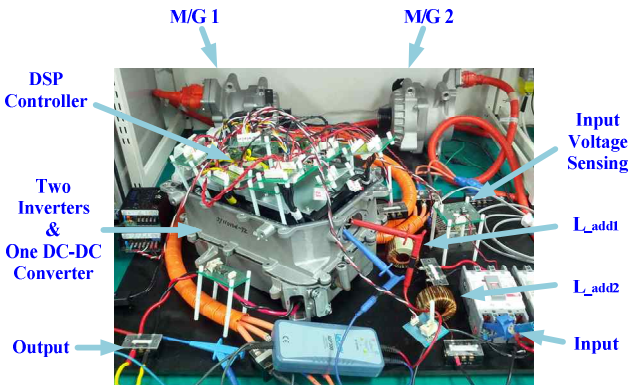

Fig. 8. Experimental setup for IBCs.

TABLE IV
SPECIFICATION OF THE EXPERIMENT

Input Voltage	220 Vac
DC-link Voltage	380 V
Output Voltage	193 V
Input Frequency	60 Hz
Switching Frequency	20 kHz

Table IV indicates the experimental conditions. Additional inductors to compensate the motor inductance are used as follows.

- Conventional IBC : two 600μH inductors
- IBC with a diode bridge : one 1.2mH inductor
- IBC with two diodes : two 1.2mH inductors

The measured key waveforms of the three IBCs at 1.7kW of output power are shown in Fig. 9. Since the same control algorithm is applied to the three IBCs and the conventional IBC also utilizes a CT for input current sensing, they are all very similar in terms of input PF and input current THD. The input PF is about 0.995 and input current THD is about 9.5%. However, the u-phase current (i_u) of M/G 1 appears in different waveforms owing to the different structures of the PFC part. From these waveforms, it can be seen that the return paths of the input current are different from one another.

Fig. 10(a) plots the measured efficiencies of the three IBCs at different output powers, from 1.2kW to 1.7kW. With an increase in the output power, the efficiencies of all of the IBCs continue to rise. The IBC with two diodes shows the highest efficiency over the whole output range. Its maximum efficiency is 81.4% at 1.7kW.

Recently, some car manufacturers introduced new PHEV models which adopt a very high voltage battery pack in order to increase the propulsion efficiency. Sometimes they do not include the HDC part. Therefore, Fig. 10(b) displays the efficiency curves for only the PFC part of each IBC system. As expected, the PFC part of the IBC with two diodes operates at the highest efficiency. Its maximum efficiency is 86.6% at 1.8kW.

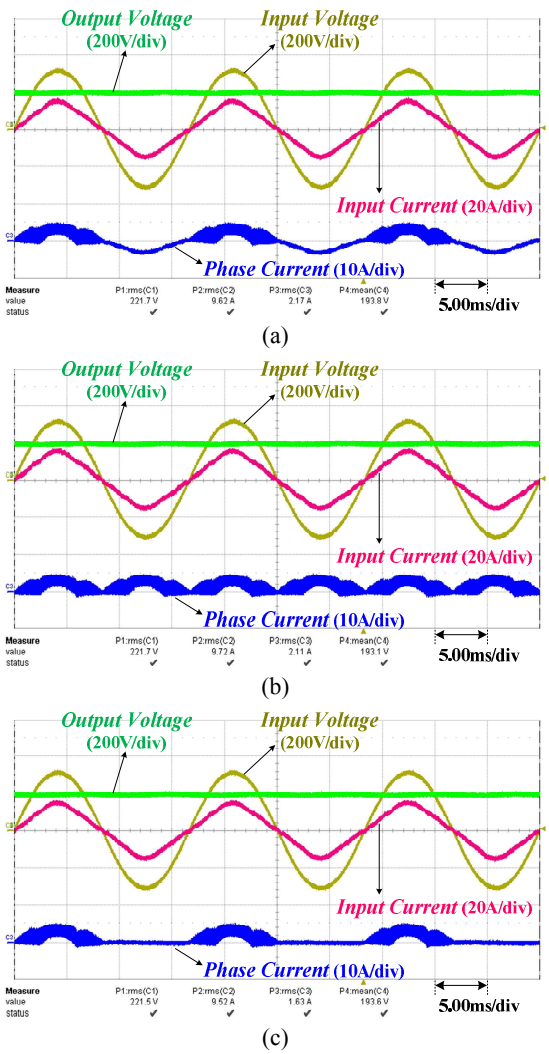

Fig. 9. Experimental waveforms at 1.7kW output power: (a) conventional IBC; (b) IBC with a diode bridge; (c) IBC with two diodes.

In both Figs. 10(a) and 10(b), the conventional IBC has the lowest efficiency because of the high conduction losses from the inverters and M/Gs. As a result, the advanced IBCs, especially the IBC with two diodes, have higher efficiencies than the conventional IBC.

VI. CONCLUSIONS

In this paper, some of the features and drawbacks of the conventional IBC for PHEVs using IPM motors are explained, and two advanced IBCs are proposed to make up for the weak points. The proposed IBC with two diodes has many advantages: 1) outstanding efficiency; 2) low CM noise; 3) simple input current sensing. The proposed IBC with a diode bridge provides a flexible structure according to the charging power as well as low CM noise, simple input voltage sensing, and simple input current sensing. Then, the average current mode control for the boost PFC operation is revised to

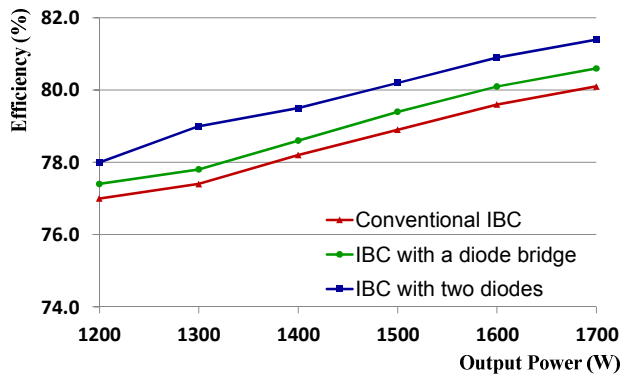

(a)

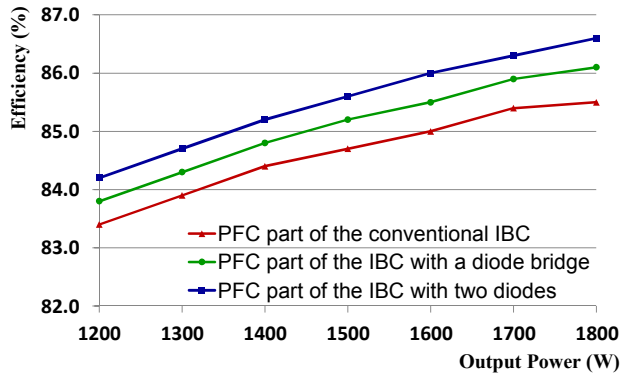

(b)

Fig. 10. Measured efficiency curves for three IBCs: (a) the whole IBC systems; (b) the PFC part of each IBC system.

enhance the system performance, and a power loss analysis on the three IBCs are performed using PSIM 9.0 simulation software. Finally, a prototype, which is composed of a 35kW inverter, a 20kW inverter, a 20kW bidirectional dc-dc converter, and 6.7kW IPM motors, is built. The experimental results obtained from the prototype verify that the IBC with two diodes achieves the highest efficiency.

ACKNOWLEDGMENT

This work was financially supported by the grant from the Industrial Strategic Technology Development Program (No. 10035276-2012-03) of the Ministry of Knowledge Economy (MKE) of Korea.

REFERENCES

[1] S. K. Sul and S. J. Lee, "An integral battery charger for four wheel drive electric vehicle," *IEEE Trans. Ind. Appl.* Vol. 31, No. 5, pp. 1096-1099, Sep./Oct. 1995.

[2] L. Solero, "Nonconventional on-board charger for electric vehicle propulsion batteries," *IEEE Trans. Veh. Technol.* Vol. 50, No. 1, pp. 144-149, Jan. 2001.

[3] L. Tang and G.-J. Su, "A low-cost, digitally-controlled charger for plug-in hybrid electric vehicles," *Proceedings of the 2009 ECCE*, pp. 3923-3929, Sep. 2009.

[4] G. Pellegrino, E. Armando, and P. Guglielmi, "An integral battery charger with power factor correction for electric scooter," *IEEE Trans. Power Electron.*, Vol. 25, No. 3, pp. 751-759, Mar. 2010.

[5] L. Tang and G.-J. Su, "Control Scheme optimization for a low-cost, digitally-controlled charger for plug-in hybrid electric vehicles," *Proceedings of the 2010 ECCE*, pp. 3604-3610, Sept. 2010.

[6] H. Ye, Z. Yang, J. Dai, C. Yan, X. Xin, and J. Ying, "Common mode noise modeling and analysis of dual boost PFC circuit," *Proceedings of the 2004 INTELEC*, pp. 575-582, Sept. 2004.

[7] B. Lu, R. Brown, and M. Soldano, "Bridgeless PFC implementation using one cycle control technique," *Proceedings of the 2005 APEC*, pp. 812-817, Mar. 2005.

[8] P. Kong, S. Wang, and F.C. Lee, "Common mode EMI noise suppression for bridgeless PFC converters," *IEEE Trans. Power Electron.*, Vol. 23, No. 1, pp. 291-297, Jan. 2008.

[9] L. Huber, Y. T. Jang, and M. M. Jovanovic, "Performance evaluation of bridgeless PFC boost rectifiers," *IEEE Trans. Power Electron.*, Vol. 23, No. 3, pp. 1381-1390, May 2008.

[10] Application Guide, "Power factor correction inductor design for switch mode power supplies using METGLAS powerlite C-cores," Matglas, Inc., Available: www.metglas.com/downloads/apps/pfc.pdf

Dong-Gyun Woo received his B.S. and M.S. in Electrical Engineering from Sungkyunkwan University, Suwon, Korea, in 2009 and 2012, respectively. Since 2012, he has been working towards his Ph.D. in Electrical Engineering at Sungkyunkwan University. His current research interests include battery chargers for PHEV/EV and renewable energy conversion systems.

Yun-Sung Kim received his B.S. and M.S. in Electrical Engineering from Cheongju University, Cheongju, Korea, in 2000 and 2002, respectively. He joined the Research and Development Center at Dongah Elecomm Corporation, Yongin, Korea, in 2002, where he has been working for the Advanced Development Team in the R&D Center as a Senior Engineer since 2004. He has been working towards his Ph.D. in Electrical Engineering at Sungkyunwan University, Suwon, Korea, since 2010. His current research interests include battery chargers for PHEV/EV, renewable energy conversion systems, and high efficiency resonant converters.

Gu-Bae Kang received his B.S. in Electronic and Electrical Engineering from Kyungpook National University, Daegu, Korea, in 1996, and his M.S. and Ph.D. in Electrical Engineering from the Pohang University of Science and Technology, Pohang, Korea, in 1998 and 2003, respectively. Since 2003, Dr. Kang has been working for the Research and Development Division, Hyundai Motor Company, Whasung, Korea.

Byoung-Kuk Lee received his B.S. and M.S. in Electrical Engineering from Hanyang University, Seoul, Korea, in 1994 and 1996, respectively, and his Ph.D. in Electrical Engineering from Texas A&M University, College Station, TX, in 2001. From 2003 to 2005, he was a Senior Researcher in the Power Electronics Group, Korea Electrotechnology Research Institute (KERI), Changwon, Korea. Since 2006 Dr. Lee has been working in the School of Information and Communication Engineering, Sungkyunkwan University, Suwon, Korea. His current research interests include chargers for electric vehicles, hybrid renewable energy systems, dc distribution systems for home appliances, power conditioning systems for fuel cells and photovoltaic applications, modeling and simulation, and power electronics. Prof. Lee was a recipient of the Outstanding Scientists of the 21st Century Award from the IBC, and he was listed in the 2008 Ed. of Who's Who in America. Prof. Lee is an Associate Editor of the IEEE Transactions on Industrial Electronics and Power Electronics. He served as the General Chair for the IEEE Vehicular Power and Propulsion Conference (VPPC) in 2012.